Thermochimica Acta, 238 (1994) 229–255
Elsevier Science B.V., Amsterdam
SSDI 0040-6031(93)1570-S

Dielectric relaxation as a probe of interphase structure

Peggy Cebe * and Peter P. Huo [1]

Materials Science and Engineering Department, Massachusetts Institute of Technology, Cambridge, MA 02139 (USA)

(Received 26 April 1993; accepted 7 September 1993)

Abstract

The electrical and thermal properties of two high-performance polymers, PEEK, poly(etheretherketone), and NEW-TPI semicrystalline thermoplastic polyimide, are reviewed and compared in this work. Dielectric relaxation was used as a probe of the crystal/amorphous interphase and is shown to be sensitive to the interphase structure in the temperature range above the glass transition. The dielectric relaxation intensity is related to the number density of dipoles that are relaxed at a given temperature. For NEW-TPI, the constrained amorphous phase is completely relaxed within thirty degrees above T_g, while for PEEK the interphase relaxes more gradually. Thermal analysis shows that PEEK contains a much larger fraction of constrained amorphous chains and a much smaller fraction of mobile amorphous chains, compared to NEW-TPI. PEEK crystallizes more rapidly above the glass transition, and a large fraction of PEEK crystallinity is attributed to secondary crystallization processes. In NEW-TPI, as a result of the increased chain stiffness, cold crystallization is slow and little or no crystals develop by secondary crystallization. These differences in crystallization behaviour of the two materials may be related to the differences in the formation of a rigid amorphous interphase.

INTRODUCTION

Failure of the two-phase model adequately to describe the morphology of semicrystalline polymers has been recognized for a long time [1–8]. The picture of perfect lamellar crystals separated by random coil-like amorphous chains was deemed too simple, and could not account for specific observations. For example, observation of a third relaxation between the amorphous and crystal phase relaxations in polyethylene [9] was attributed to the fold surface region which exhibited properties intermediate between those of the crystal and amorphous phases. Such a region may generally be

* Corresponding author.
[1] Present address: W.R. Grace Corp., Analytical Division, Columbia, MD, USA.

termed an "interphase", or transition zone, over which a variation in properties occurs. Other examples of systems which may possess an interphase would include block copolymers, fiber/matrix composites, immiscible and partially miscible blends, blends with one component crystallizable, semi-interpenetrating networks, and polymers containing additives such as toughening agents.

In this paper, we review our recent work using dielectric relaxation to explore the molecular mobility of interphase regions [10–12]. In Fig. 1, a very simple sketch of three regions is shown. The regions differ in their molecular mobility, with region 1 being the most rigid, and 2 the least rigid. Region i is the interphase, and has intermediate mobility. To probe the temperature-dependent relaxation, we utilize a local probe of molecular mobility, here shown as an arrow. In the case of dielectric experiments, the arrow is an electric dipole of dipole moment μ. In a different type of experiment using nuclear magnetic resonance, the arrow is a nuclear magnetic dipole moment. We have used both approaches in our study of molecular mobility in poly(phenylene sulfide), PPS [10, 13]. Here we restrict our attention to the electric dipole probe, which we have previously used to study molecular mobility in two other high-performance polymers, poly(etheretherketone), PEEK [11], and the semicrystalline polyimide, NEW-TPI [12]. While in some cases the probe itself may be an additive, for example a dopant molecule which has a dipole moment, in our studies the electric dipole is located on the polymer chain and is controlled by the chemistry of the monomer repeat unit. In Fig. 1, if regions 1, 2 and i are chemically the same, e.g. a homopolymer, then differences in behaviour of the electric dipole probe can be related directly to the differences in molecular mobility among the three regions at any temperature.

In this work, we consider specifically the interphase region which exists in semicrystalline polymers as a result of the constraining effect of crystals

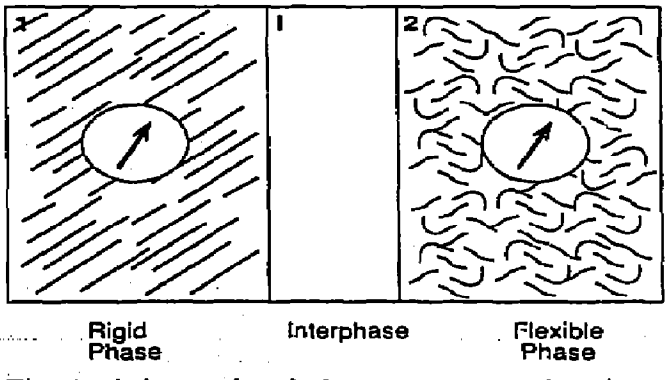

Fig. 1. Schematic of phase structure showing more and less mobile regions separated by an interphase. The arrow represents a local probe of mobility, such as an electric dipole moment or a nuclear magnetic moment.

on the mobility of the amorphous phase. This interphase material has been termed the rigid amorphous phase fraction [14–20], or the constrained amorphous phase. We describe the dielectric relaxation method which allowed us quantitatively to analyze the mobility of such interphase regions as a function of temperature [10–12]. We compare the dielectric method to thermal analysis methods which have been used to deduce the existence of rigid interphase material [14–20]. Finally, we consider the possible relation ship between chemical structure differences and effects of the kinetics of crystallization in two systems which are shown to exhibit very different relaxation behavior of the interphase. The two polymers that will be compared here are PEEK and NEW-TPI thermoplastic polyimide. Our results lead to a general picture which suggests that polymers that crystallize slowly, and with little or no formation of secondary crystals, will have smaller amounts of low-mobility interphase. Polymers that crystallize rapidly, and form large populations of secondary crystals, may force large constraints upon the amorphous phase leading to formation of a significant amount of constrained interphase.

THEORETICAL SECTION

In this section, we review the basis for the use of dielectric relaxation to study interphases. The dielectric relaxation intensity is shown to be related to the dielectric constant and loss, which are the experimentally measured quantities. Then the relaxation intensity is related to the microscopic parameters of interest, namely the number density of the relaxing dipoles. These concepts are summarized from various excellent reviews, to which the reader is referred for greater detail [21–25].

Dielectric relaxation intensity

The complex dielectric function, $\hat{\varepsilon} = \varepsilon' - i\varepsilon''$, is obtained by direct measurement (as described in the Experimental Section below) as a function of frequency and temperature; $\hat{\varepsilon}$ can be written according to the Havriliak–Negami formulation [26] of the Debye equations [27] as

$$\hat{\varepsilon} = \varepsilon_\infty + \frac{(\varepsilon_s - \varepsilon_\infty)}{[1 + (i\omega\tau)^{a_1}]^{a_2}} \tag{1}$$

The parameters a_1 and a_2 ($0 < a_i < 1$) are empirical broadening factors that describe the departure from the Debye equations for which $a_1 = a_2 = 1$. In eqn. (1), ω is the angular frequency of the applied field, τ is the central relaxation time for the process of interest, and ε_∞ and ε_s are the high and low frequency limiting values of the permittivity, respectively. In the case where the broadening is symmetric, which was in fact the case for our investigations of PPS, PEEK, and NEW-TPI [10–12], then $a_2 = 1$. Under

the condition $a_2 = 1$, the set of equations given by eqn. (1) can be rewritten as [28]

$$\varepsilon' = \varepsilon_\infty + (\varepsilon_s - \varepsilon_\infty)\left[\frac{1 + (\omega\tau)^{a_1}\cos(a_1\pi/2)}{1 + 2(\omega\tau)^{a_1}\cos(a_1\pi/2) + (\omega\tau)^{2a_1}}\right] \tag{2a}$$

$$\varepsilon'' = (\varepsilon_s - \varepsilon_\infty)\left[\frac{(\omega\tau)^{a_1}\sin(a_1\pi/2)}{1 + 2(\omega\tau)^{a_1}\cos(a_1\pi/2) + (\omega\tau)^{2a_1}}\right] \tag{2b}$$

These equations can be solved to eliminate the common variable, $\omega\tau$, and the resulting equation is that of a circle in the complex plane given by [28]

$$\left(\varepsilon' - \frac{\varepsilon_s + \varepsilon_\infty}{2}\right)^2 + \left(\varepsilon'' + \frac{\varepsilon_s - \varepsilon_\infty}{2}\operatorname{ctn}\left(a_1\frac{\pi}{2}\right)\right)^2 = \left(\frac{\varepsilon_s - \varepsilon_\infty}{2}\operatorname{csc}\left(a_1\frac{\pi}{2}\right)\right)^2 \tag{3}$$

A plot of ε'' versus ε' is called a Cole–Cole plot [28]. The intersection points of the circle with the axis $\varepsilon'' = 0$ give the values of ε_∞ and ε_s directly. The difference $\varepsilon_s - \varepsilon_\infty$ is called the relaxation intensity, or relaxation "strength".

Relationship to microscopic parameters

Many excellent reviews derive the relationship between macroscopic quantities, such as the dielectric relaxation strength, $\varepsilon_s - \varepsilon_\infty$, and microscopic parameters characterizing the dipoles on a polymer chain [21–25]. The main factors which need to be considered include first, the temperature dependence of the orientational polarizability, α_0, which has the general form

$$\alpha_0 = N\mu^2/3kT \tag{4}$$

where N is the number of dipoles per unit volume, μ is the dipole moment, k is Boltzmann's constant, and T is temperature. Next, on a polymer chain, the orientation of any dipole unit will be correlated to that of neighboring dipoles on the same chain because of hindered rotations. Finally, the applied electric field will differ from the electric field acting locally at the position of the dipole. Using the formulation of Frohlich [21], the limiting static dielectric constant difference at temperature T can be written

$$\varepsilon(T)_s - \varepsilon(T)_\infty = \frac{N_r\mu_r^2}{3\varepsilon_0 kT}(3\varepsilon_s)\frac{(2\varepsilon_s + \varepsilon_\infty)}{(2\varepsilon_s + 1)^2}\left[1 + \sum_{k',k\neq k'}\langle\cos\theta_{kk'}(0)\rangle\right] \tag{5}$$

where μ_r is the dipole moment of a repeat unit and N_r is the number of dipole groups (repeat units) per unit volume. The last term, in square brackets, reflects the angular correlation between dipoles k and k' on the same chain. A similar term could be included for the angular correlation between dipoles on different chains, but for polymers this may be considered as negligible [22]. The two middle terms containing ε_s and ε_∞ arise from the Onsager relationship of the local to the applied electric field [29]. It is our specific interest to consider the temperature dependence of the dielectric response. Rewriting eqn. (5) to collect terms in ε_s and ε_∞ we have

$$\frac{\varepsilon(T)_s - \varepsilon(T)_\infty}{\mathscr{F}(T)} = N(T)_r g(T)\left(\frac{\mu_r^2}{3\varepsilon_0 kT}\right) \tag{6}$$

For simplification, in eqn. (6) we have used g for the angular correlation term, and $\mathscr{F}$ for the electric field ratio which is defined as

$$\mathscr{F} = \frac{(3\varepsilon_s)(2\varepsilon_s + \varepsilon_\infty)}{(2\varepsilon_s + 1)^2} \tag{7}$$

Equation (6) was derived on the assumption that the material is homogeneous, which is a reasonable assumption for the case of a quenched amorphous polymer. For a semicrystalline material, the representation of the polymer as a mixture of separate phases has been treated in detail by Boyd [30]. In our relaxation study, we are concerned with the amorphous phase relaxation only. At the temperatures and frequencies of interest, the crystals are dielectrically inactive. The crystals act as constraints on the mobility of the amorphous phase but the specific morphology of the crystals is not taken into account.

EXPERIMENTAL SECTION

Electrical measurements

Here we describe in detail our experimental setup which was used in our research reported previously [10–13]. These details have not been presented elsewhere. First, the polymer film is coated on both sides with thermally evaporated gold electrodes. During the evaporation process, the film is heat-sunk to a metal block to avoid any temperature increase. The gold layer provides very intimate contact with the sample surface and prevents the introduction of any air gap. The area of the gold coating

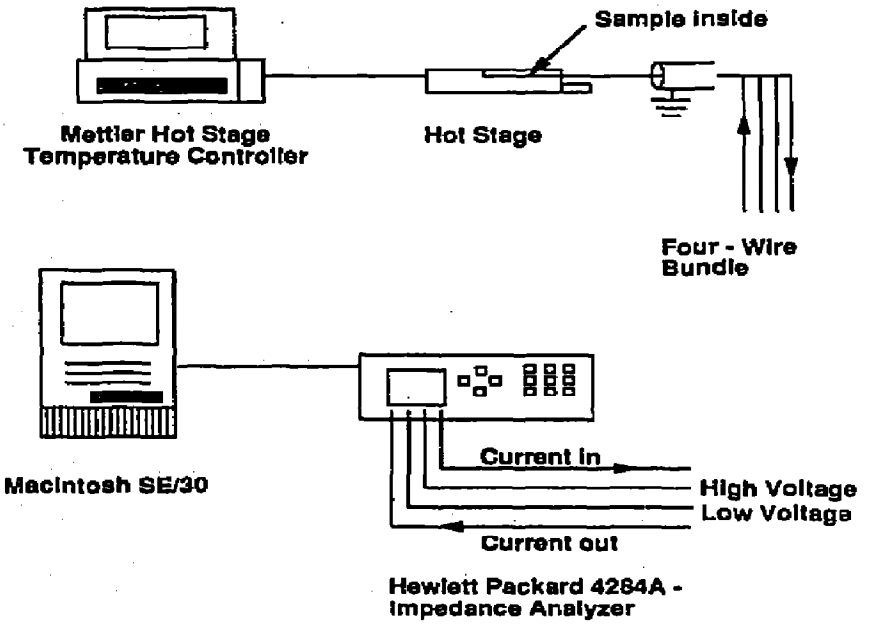

Fig. 2. Experimental setup for dielectric relaxation experiments showing computer control of impedance analyzer and hot stage for temperature control. The four-wire bundle is attached to rigid electrodes between which the sample film is placed.

defines the area used in the calculation of the dielectric function. Two rigid brass disk electrodes are then positioned against the polymer film surface and held in place by Kapton™ tape. The surface area of the brass disks is slightly less than the surface area of the sample coated by the gold. This allows easy positioning of the electrodes. The upper brass disk is connected to the high voltage supply and current-in wires; the lower brass disk is connected to the low voltage and current-out wires. In our situation, the electrode radius (5.0 mm) is very much greater than the film thickness (0.075 mm), so that the effect of fringe fields is negligible. Therefore, we did not employ a guard electrode.

The measurement system is shown in Fig. 2. The main components include: temperature control system, voltage and current measurement system, data collection and analysis system, and the sample electrode assembly described above. The temperature control functions are handled by a Mettler FP80 microscope hot stage and its controller, which can either heat at a constant rate or hold isothermally. The practical temperature range is from room temperature up to about 320°C. The heating rate used was 1–2°C min^{-1}. The hot stage was slightly modified by filing away the entrance slot to make it wider; this allows the somewhat thick electrode assembly to be placed inside the stage without opening the stage cover.

The voltage and current supply and measurement are handled by a Hewlett Packard 4284A Precision LCR meter. Corrections are made for

open and short circuit conditions. The frequency range of this instrument is from 100 Hz to 1 MHz, but in practice we did not use frequencies below 500 Hz because the lower frequency signal-to-noise ratio was unfavorable, and ionic conductivity effects increase greatly as frequency is reduced. Data collection and analysis tasks are handled by a Macintosh SE30 computer with a National Instruments board and Labview™ software. Data from the HP impedance analyzer are fed directly into the computer upon execution of a manual "start" signal. The system measures the capacitance C_p and resistance R_p of an equivalent circuit modeled as a parallel combination. The real and imaginary parts of the dielectric function are determined from the measured quantities according to

$$\varepsilon' = C_p/C_0 = C_p d/(A\varepsilon_0) \tag{8a}$$

$$\varepsilon'' = 1/(R_p C_0 \omega) = d/(R_p A \varepsilon_0 \omega) \tag{8b}$$

where C_0 is the empty cell capacitance, d is the initial film thickness and A is the electrode area. Eliminating the geometrical factors, we define the loss tangent as $\tan\delta = \varepsilon''/\varepsilon'$.

The real and imaginary parts of the dielectric function are analyzed according to eqn. (3) using a non-linear least-squares fitting routine [31]. The fitting parameters were $(\varepsilon_s - \varepsilon_\infty)/2$, ε_∞ and a_1. Not all the data points were used in the fitting. Ionic conductivity effects (at low frequency) and overlap of secondary relaxations (at high frequency) occasionally resulted in a data point being excluded from the fit. To determine whether a point would be excluded, a cubic spline fit to the data was made and the second derivative evaluated. A change of sign of the second derivative was used as the determining factor. The validity of the fitting procedure used to determine the intercepts $\varepsilon(T)_s$ and $\varepsilon(T)_\infty$ was checked in the following way. First, the parameter $(\varepsilon_s - \varepsilon_\infty)/2$ was forced to take a value that deviated from its best fit value. The fitting program was rerun with $(\varepsilon_s - \varepsilon_\infty)/2$ fixed at this new value, and with ε_∞ and a_1 now free to take values as needed to minimize the squared deviations of the calculated ε'' from the ε'' data. The fit was judged to be poor as soon as the initial choice resulted in a factor of two change in the chi-square value. This criterion was applied to each of the fit parameters in turn. Results indicate that the value of $(\varepsilon_s - \varepsilon_\infty)/2$ is determined to ±4%, ε_∞ to ±0.5%, and a_1 to ±5%.

Sample characterization

Two polymers are compared in the present study, PEEK and NEW-TPI. The chemical structure of PEEK is well known [32], and contains alternating phenyl–ether and phenyl–ketone linkages. PEEK polymer was

obtained in pellet form from ICI Americas, Inc. and compression-molded into thin sheets as previously described [33]. During molding the films were heated to 370°C, then an amorphous film was made by quenching from the melt into ice water. The glass transition of the amorphous film was determined to be 145°C, from the midpoint of the sigmoidal transition, during scanning in a Perkin-Elmer DSC-4 at 20°C min^{-1}. Crystalline film was made by rapidly heating the amorphous film in a Mettler FP80 hot stage to a cold crystallization temperature above T_g and holding for 1 h. The crystalline film was removed from the hot stage and allowed to cool in air to room temperature.

NEW-TPI (product of Mitsui Toatsu) is a recent addition to the family of polyimides. Its chemical structure has been previously published [34–36] and is shown in Scheme 1.

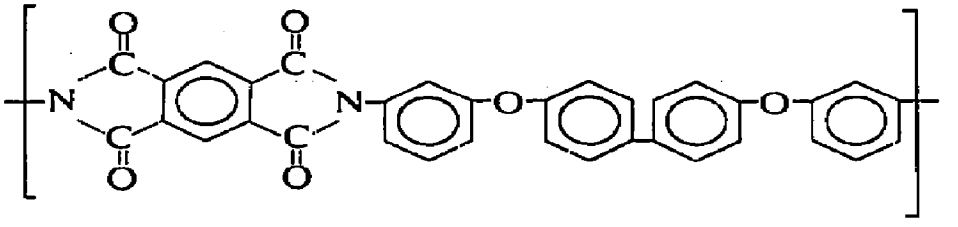

Scheme 1. The structure of NEW-TPI.

This polymer is composed of a very rigid dianhydride component, made from pyromellitic dianhydride, PMDA. This group imparts a high degree of chain rigidity to NEW-TPI. To make NEW–TPI both crystallizable and thermoplastic, flexibilizing groups are incorporated into the diamine component. NEW-TPI film was processed by Foster Miller, Inc. from NEW-TPI pellets provided by Mitsui Toatsu Chemical Co. and now marketed as Aurum™. The as-received film was amorphous, judging from wide-angle X-ray scattering curves, and the equality of heats of crystallization and melting [35]. The glass transition temperature, determined as above, was 248°C. Crystalline NEW-TPI film was made by rapidly heating the amorphous film in the Mettler hot stage to a cold crystallization temperature above T_g and holding for one hour. The film was cooled by quenching in air.

Thermal analysis was performed on all materials using a Perkin-Elmer DSC-4 with a 20°C min^{-1} scanning rate. The sample masses were in the range from 2 to 10 mg. The heats of reaction, glass transition, and melting temperatures were calibrated using indium and tin standards. The melting points were determined from the peaks of the melting endotherms. The degree of crystallinity χ_c was determined from area of the fusion peak, using 130 J g^{-1} for PEEK [32] and 139 J g^{-1} for NEW-TPI [37]. The use of thermal analysis to determine the amount of interphase material has been

described previously [10–12, 14]. The interphase, being of reduced molecular mobility, has been termed the "rigid amorphous fraction" or the constrained amorphous fraction. The amount of rigid amorphous interphase material as measured thermally is designated χ_{ra} and is found from

$$\chi_{ra} + \chi_c + \chi_a = 1 \tag{9}$$

where χ_a is the amount of amorphous phase which exhibits a clear heat capacity step at the glass transition temperature [10–12, 14–20] and is found from the ratio between the glass transition heat capacity increment of the semicrystalline polymer and the increment in the 100% amorphous polymer.

RESULTS

Thermal analysis

The phase composition of the two polymers is compared in Fig. 3(a) and (b) for PEEK and NEW-TPI, respectively. In both polymers, the mass

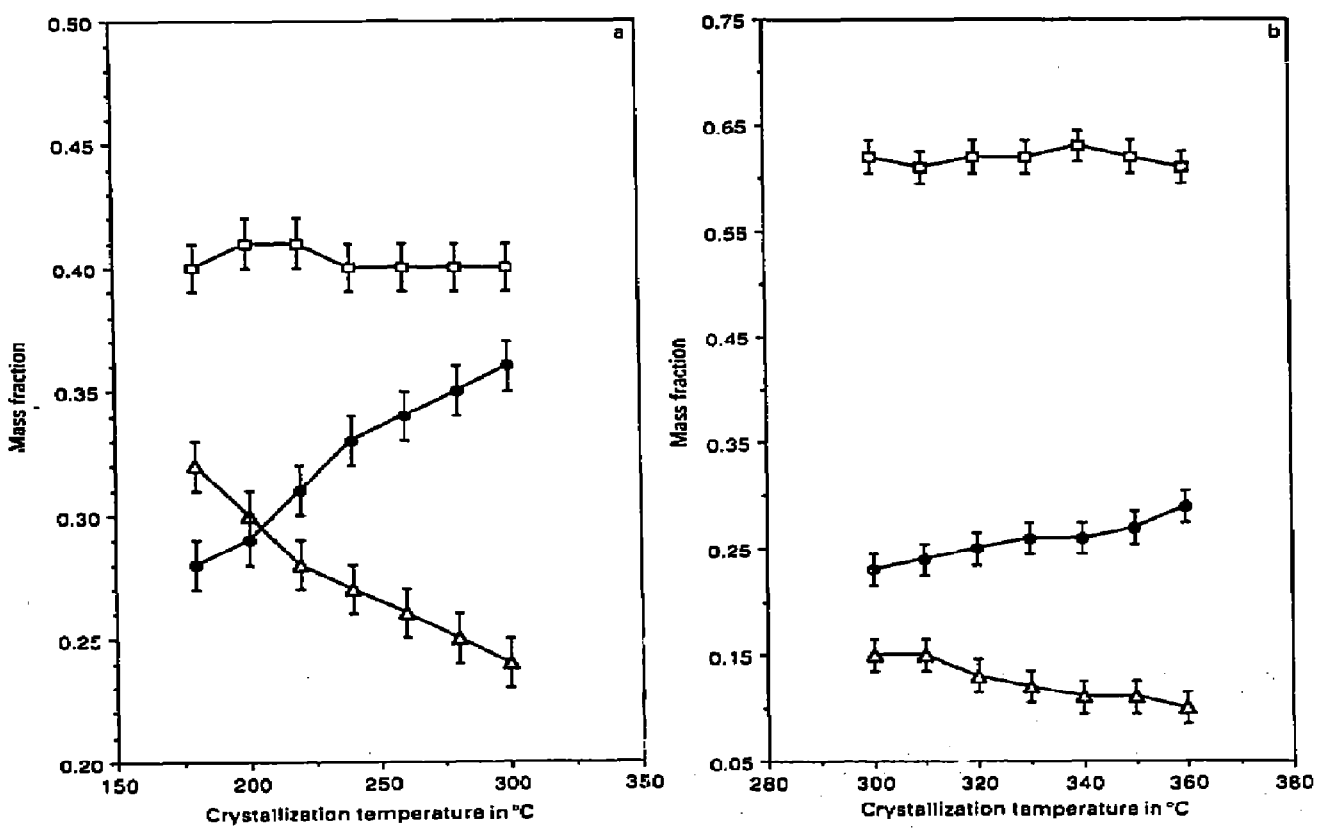

Fig. 3. Mass fractions of the three phases as a function of cold crystallization temperature: ●, crystal phase; □, liquid-like amorphous phase; and △, rigid amorphous phase. (a) PEEK. (b) NEW-TPI.

fraction crystallinity (solid circles) increases as a function of crystallization temperature while the liquid-like, or more mobile amorphous fraction, (open squares) is relatively insensitive to thermal treatment. The rigid amorphous fraction (open triangles) is calculated from eqn. (9). As a function of crystallization temperature, this fraction decreases in both polymers. The degree of crystallinity for PEEK is slightly larger than for NEW-TPI. For the PEEK samples, χ_c is in the range 0.28–0.36, which is quite typical for this polymer [32, 33, 38]. NEW-TPI has a slightly smaller degree of crystallinity, at about 0.25, which is also typical [35, 36]. NEW-TPI has a much larger liquid-like amorphous phase (0.60) compared to PEEK (0.40); NEW-TPI has a much smaller rigid amorphous phase (0.15–0.10) compared to PEEK (0.32–0.24).

Table 1 shows the thermal analysis results for PEEK and NEW-TPI for the cold crystallization treatments described in the Experimental section. The glass transition temperatures and DSC melting points were found from the DSC scans of films heated from room temperature to above the melting

TABLE 1

Thermal properties at 20°C min^{-1} of PEEK and NEW-TPI: glass transition and melting peak temperatures of amorphous films and of films cold-crystallized at the indicated temperatures

Crystallization temp./°C	T_g/°C (±0.3°C)	T_{m1}/°C (±0.3°C)	T_{m2}/°C (±0.3°C)
PEEK			
Amorphous [a]	145.1	– [b]	335
180	159.1	199.7	337.8
200	158.5	223.4	337.8
220	158.0	242.8	338.4
240	157.6	261.6	338.4
260	156.8	277.8	338.4
280	155.7	297.8	337.8
300	154.8	318.5	338.5
NEW-TPI			
Amorphous [a]	248	– [b]	382
300	252.9	314.4	381.5
310	251.3	321.9	380.3
320	250.0	332.5	379.5
330	248.7	340.9	380.9
340	247.3	351.0	381.9
350	246.5	360.5	385.0
360	244.4	371.8	389.4

[a] Amorphous films were quenched from above the infinite crystal melting point to 25°C. [b] No dual melting point observed.

endotherm at 20°C min^{-1}. Cold crystallization was chosen because it has been previously shown to result in the largest amount of rigid amorphous fraction [10, 11, 19, 20]. By these indicators, NEW-TPI is accounted as possessing the more rigid structure compared to PEEK. Amorphous PEEK has a T_g value of 145°C [11, 32] while amorphous NEW-TPI has a T_g of 248°C [35, 36]. The DSC melting points also indicated the more rigid chemical structure of NEW-TPI. The upper melting point (of the dual endotherms usually seen) is near 338°C for PEEK [32, 33, 38] and 380°C for NEW-TPI [35, 36].

Generally, it is expected that the crystals act as constriants, or thermoreversible crosslinks, which reduce the mobility of the amorphous chains. The anticipated effect on the glass transition is that T_g is shifted to higher temperature and the temperature interval of the glass-to-rubber transition is broadened. For PEEK polymer, Table 1 shows the typical behavior in the semicrystalline polymer compared to the quenched amorphous film. Whereas the T_g of quenched PEEK is about 145°C, the T_g of all semicrystalline PEEK is nearly 10–14°C higher. The semicrystalline PEEK shows a decrease in the value of T_g as the cold crystallization temperature increases. NEW-TPI, however, has a very minor change in glass transition temperature after cold crystallization. The increase in T_g for the semicrystalline sample with $T_c = 300$°C is only 5°C. As the cold crystallization temperature increases, T_g decreases in NEW-TPI just as in PEEK. But judging by the midpoint of the step in the heat capacity, the T_g values of some semicrystalline films (those with cold crystallization temperatures greater than 330°C) are actually less than that of the quenched amorphous material.

To address the differences in crystallization behavior between PEEK and NEW-TPI, we show results of non-isothermal crystallization in Fig. 4. DSC scans of amorphous PEEK and NEW-TPI at 10°C min^{-1} over the same temperature range are shown in Fig. 4. The non-isothermal crystallization of PEEK occurs very quickly as the polymer is heated above T_g, and the exotherm and subsequent endotherm are well separated. NEW-TPI crystallizes much more slowly during heating. Above T_g, the exotherm is very broad and nearly overlaps with the start of the endotherm at this scan rate [35].

In Fig. 5, results of isothermal cold (PEEK and NEW-TPI) or melt (PEEK only) crystallization kinetics studied of these polymers are shown. While melt crystallization was not used to prepare PEEK samples for the dielectric analysis, it is presented here along with cold crystallization to show differences in the mechanism of crystallization of the two polymers. In Fig. 5, the Avrami analysis [39, 40] double logarithmic plot of crystallinity development with time is shown. For PEEK, a very large fraction of the crystals, about 0.50 relative crystallinity, develops by secondary crystallization processes [33]. This is seen by the break in the slope of the double

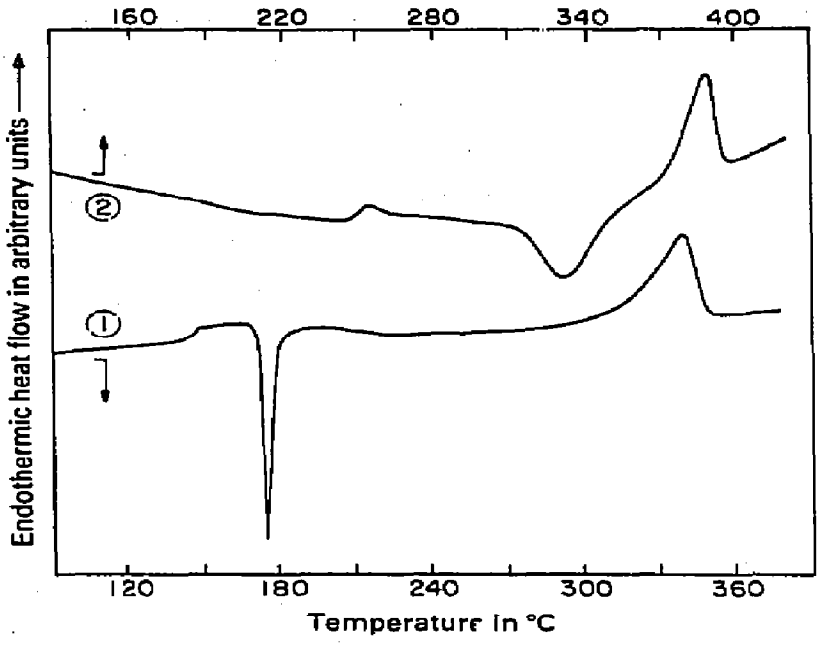

Fig. 4. Thermograms of PEEK (curve 1) and NEW-TPI (curve 2) scanned at 10°C min $^{-1}$. Heat flow has been normalized per unit of sample mass, and curves have been displaced vertically for clarity.

logarithmic plot. (Reference to the Avrami analysis of these polymers can be found in refs. 33 and 36.) For NEW-TPI, however, there is almost no break in slope at the later crystallization time, indicating that this polymer crystallizes by a single mechanism from initiation up to completion of crystallization.

Dielectric analysis

Figure 6 shows tan δ plotted against temperature for amorphous PEEK (squares) and NEW-TPI (circles), at 1 kHz (open symbols) and 100 kHz (solid symbols). Note that the vertical and horizontal scales are the same but the axes zeros have been offset for clarity and ease of comparison. Both polymers display a distinct peak at the glass transition temperature. Considering PEEK polymer, we see that at both frequencies two relaxation peaks exist, the second lower in magnitude and shifted up in temperature. At temperatures above 200°C, ionic conductivity and Maxwell–Wagner interfacial polarization effects serve to increase the loss at the lower frequency. The NEW-TPI amorphous films display a much lower loss value at the glass transition than the PEEK films. Two relaxation peaks cannot be separately distinguished in NEW-TPI amorphous film.

Semicrystalline PEEK (squares) and NEW-TPI (circles) loss tangent versus temperature plots are shown in Fig. 7 at two frequencies, 100 kHz,

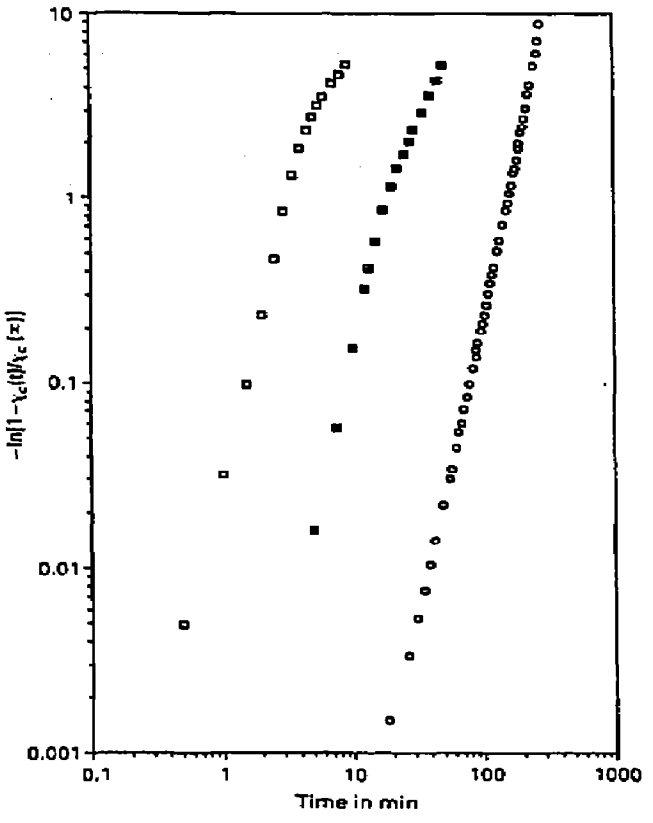

Fig. 5. Avrami plots of $\log[-\ln(1-\{\chi_c(t)/\chi_c(\infty)\})]$ vs. log time during isothermal crystallization: ■, PEEK, 315°C; □, PEEK, 164°C; ○, NEW-TPI, 340°C.

and 1 kHz (PEEk) or 2 kHz (NEW-TPI). The loss tangents are much smaller in the semicrystalline samples compared to the amorphous samples shown in Fig. 6 due to the reduction in the amount of amorphous chains. Now only one relaxation peak is seen, and its position is identical to that of the second, higher temperature peak seen in Fig. 6, which appeared after the amorphous sample crystallized.

Cole–Cole plots of ε'' versus ε' as a function of measurement temperature are shown in Fig. 8(a) and (b), respectively, for the amorphous films of PEEK [11] and NEW-TPI [12]. Symbols represent the measured data and the solid line is the best fit to eqn. (3). The interval between the x-axis intercepts represents the dielectric strength and shows an initial decreasing trend with temperature for PEEK (Fig. 8(a)). PEEK begins to crystallize (above 165°C) and after crystallization there is a sudden decrease in both intercepts. It takes about 12 s to accumulate data at all the frequencies. Within a window of about 8°C, from 166 to 174°C, crystallization is occurring so rapidly that the low and high frequency data represent different physical states of the sample. This situation results in a severe skewing of the Cole–Cole arc, and we do not attempt to analyze the

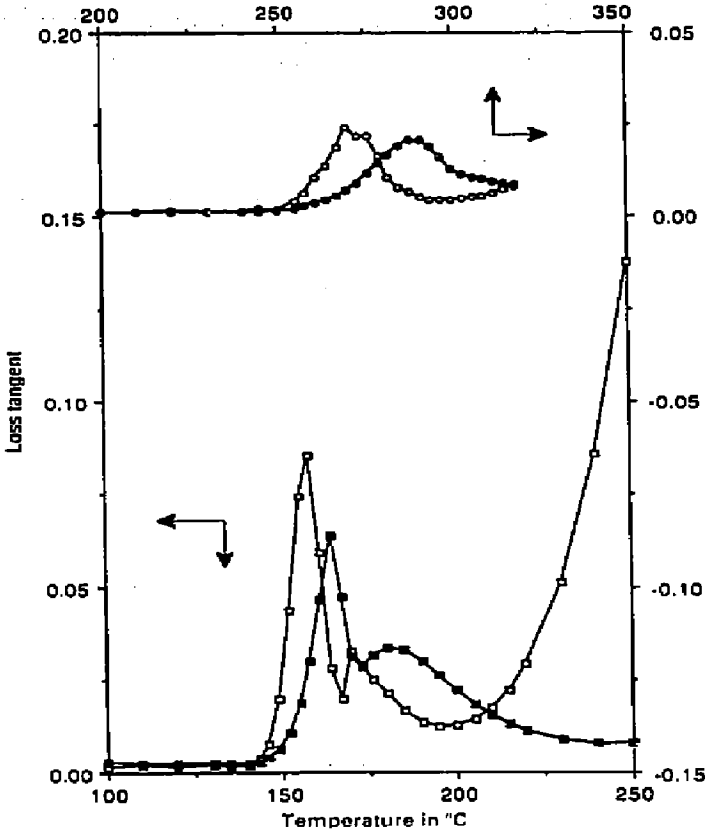

Fig. 6. Loss tangent (tan δ) vs. temperature for amorphous PEEK (□, ■) and amorphous NEW-TPI (○, ●) at frequencies of 1 kHz (open symbols) and 100 kHz (solid symbols).

relaxation strength during this period of crystallization. Following the crystallization, the relaxation strength increases for PEEK. For NEW-TPI (Fig. 8(b)), the amorphous film relaxation strength shows a monotonically decreasing trend over the entire temperature range.

The limiting values of the dielectric constants, ε_s and ε_∞, are shown in Fig. 9(a) and (b) for semicrystalline and amorphous PEEK, respectively. In Fig. 9(a), two different crystallization treatment conditions are compared. The value of ε_∞ is unchanged by the crystallization temperature. The value of ε_s is systematically larger in the PEEK sample crystallized at lower temperature. The amorphous PEEK sample is shown in Fig. 9(b). At this heating rate, the amorphous film crystallizes during heating above 165°C [11]. A change in both ε_s and ε_∞ is observed at this temperature. After crystallization, the value of ε_∞ is the same as that seen in the semicrystalline samples (Fig. 9(a)). The value of ε_s is largest prior to crystallization, and decreases suddenly from 4.5 to about 4.0 after crystallization. This value is

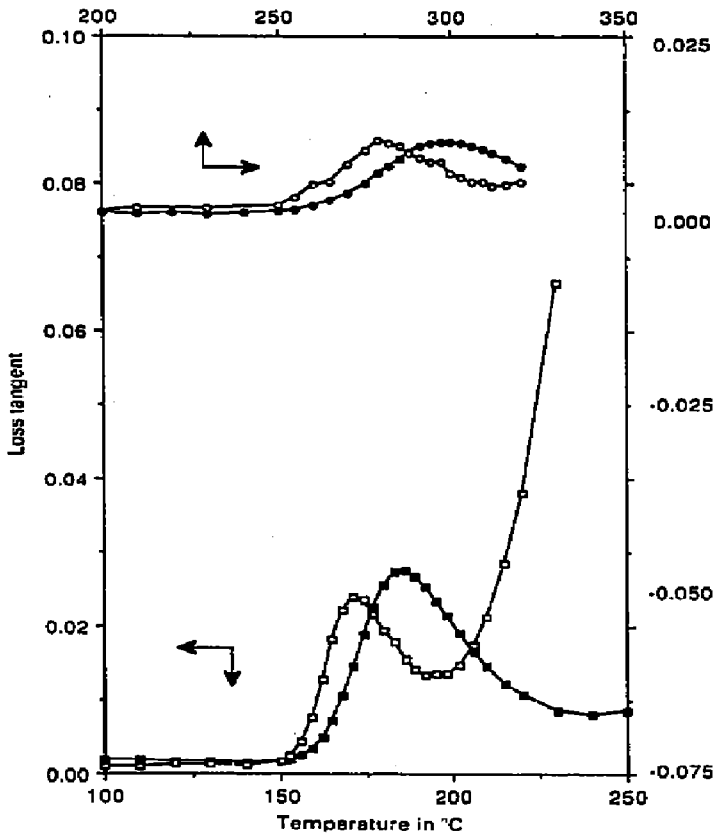

Fig. 7. Loss tangent (tan δ) vs. temperature for PEEK crystallized at 200°C (□, ■) and NEW-TPI crystallized at 300°C (○, ●) at frequencies of 1 kHz (□), 2 KHz (○), and 100 kHz (■, ●).

larger than the corresponding ε_s values seen in either of the isothermally crystallized PEEK films.

The limiting values of dielectric constant for amorphous and crystallized NEW-TPI are shown together in Fig. 10. The vertical scale is the same as that used for the semicrystalline PEEK films, shown in Fig. 9(a). The crystalline NEW-TPI sample (circles) shows a weak declining trend in both ε_s and ε_∞ which is is within the error bars. The amorphous sample (squares) also has both ε_s and ε_∞ decreasing slightly with increasing temperature and this is also within the error limits.

Figure 11(a) and (b) shows plots of the temperature dependence of the relaxation strength divided by the electric field ratio, or $(\varepsilon_s - \varepsilon_\infty)/\mathcal{F}$, for amorphous and semicrystalline samples of the two polymers. In Fig. 11(a), for two semicrystalline PEEK samples (circles), $(\varepsilon_s - \varepsilon_\infty)/\mathcal{F}$ is seen to increase with increasing temperature. For amorphous PEEK (squares), $(\varepsilon_s - \varepsilon_\infty)/\mathcal{F}$ initially decreases and then increases above 175°C. The broken

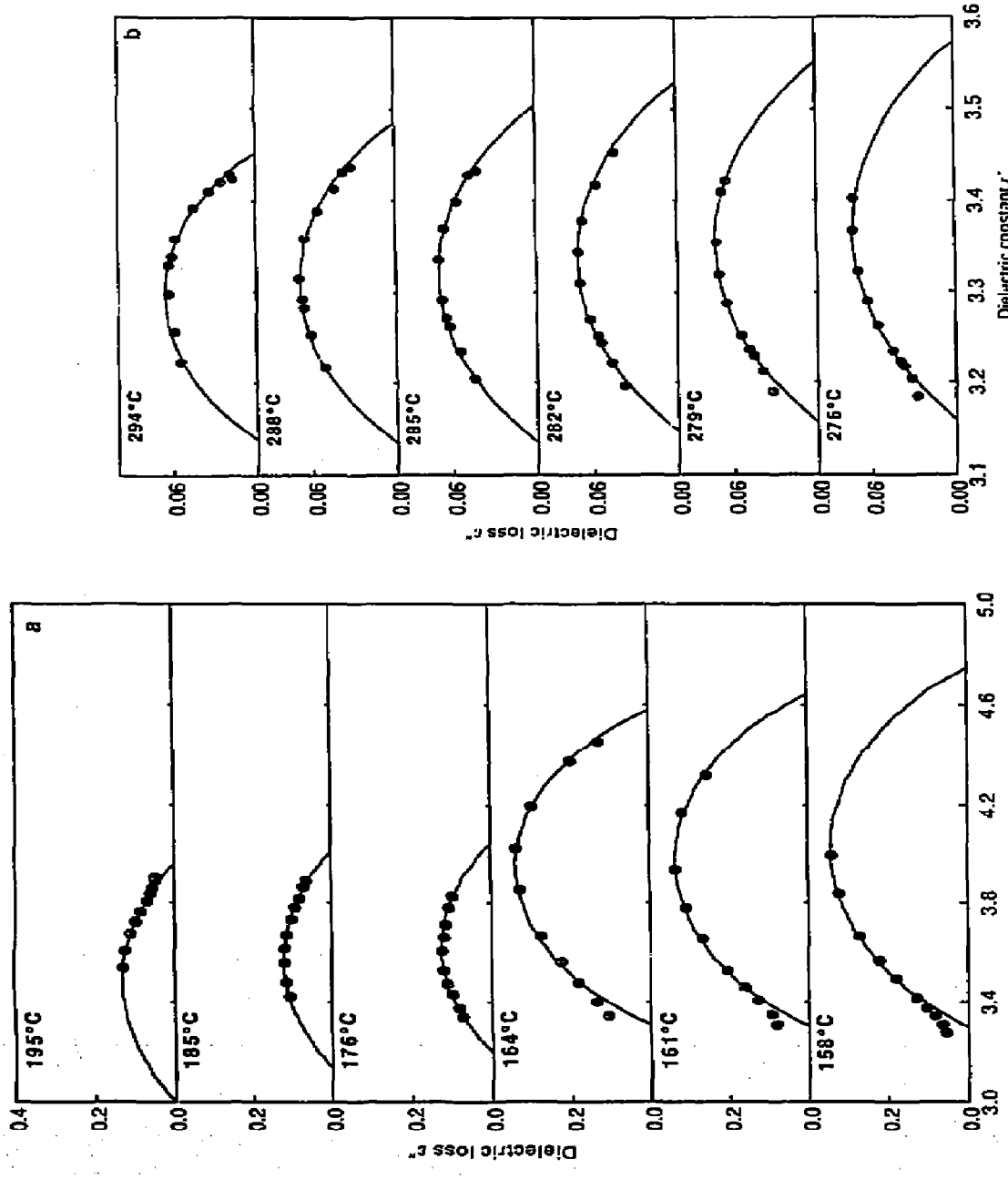

Fig. 8. Cole–Cole plots of ε'' vs. ε' at different measurement temperatures. (a) Amorphous PEEK. (b) Amorphous NEW-TPI.

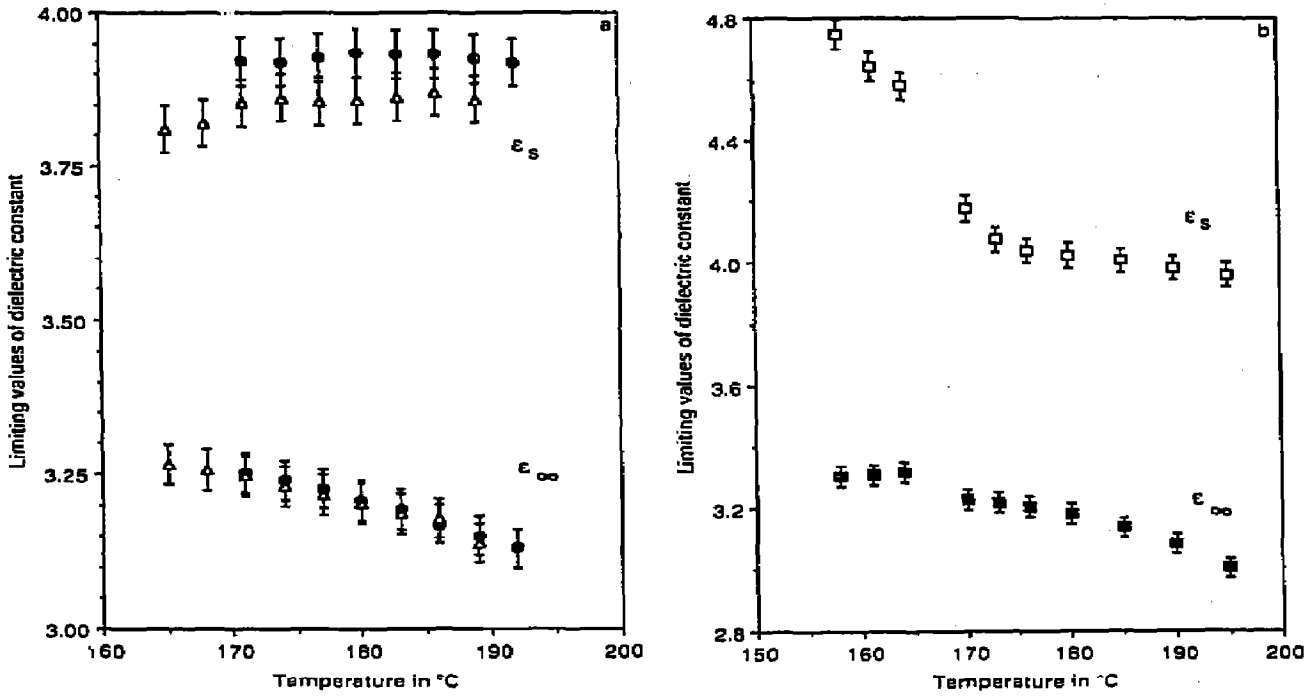

Fig. 9. Limiting values of the dielectric constant, ε_s (upper curves) and ε_∞ (lower curves), vs. temperature for PEEK. (a) Crystallized at 200°C (●) or 280°C (△). (b) Amorphous PEEK.

line represents an estimate of the behavior of non-crystallizable PEEK. For NEW-TPI shown in Fig. 11(b), the plot of $(\varepsilon_s - \varepsilon_\infty)/\mathcal{F}$ versus T for crystalline sample (solid symbols) first decreases and then levels off. The amorphous sample decreases continuously.

DISCUSSION

Thermal properties

Thermal analysis is often used as a major tool to study the properties of semicrystalline polymers. The two polymers considered here, PEEK and NEW-TPI, are shown by thermal analysis to differ in the following properties: effect of crystals on the glass transition temperature, isothermal and non-isothermal crystallization kinetics, mechanism of crystallization, amount of liquid-like amorphous phase, and amount of constrained amorphous phase. NEW-TPI has the more rigid chemical repeat unit, and as a result has slower kinetics when cold crystallizing either isothermally or non-isothermally, as shown in Fig. 2.

The process of crystal development has been analyzed by the Avrami equation [39, 40] (Fig. 4) and PEEK has a distinct change in kinetic process during the latter stages of crystallization. This leads to a decrease in the

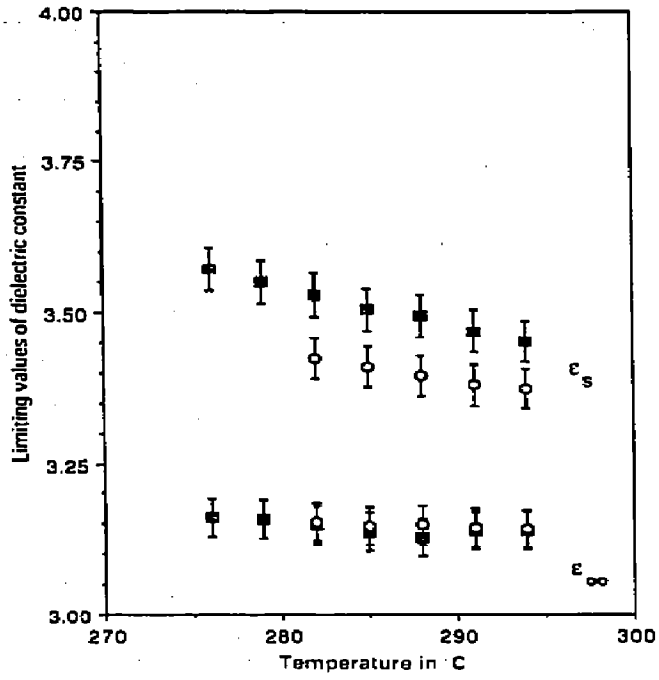

Fig. 10. Limiting values of the dielectric constant, ε_s (upper curves) and ε_∞ (lower curves), vs. temperature for NEW-TPI: ○, crystallized at 300°C: ■, amorphous.

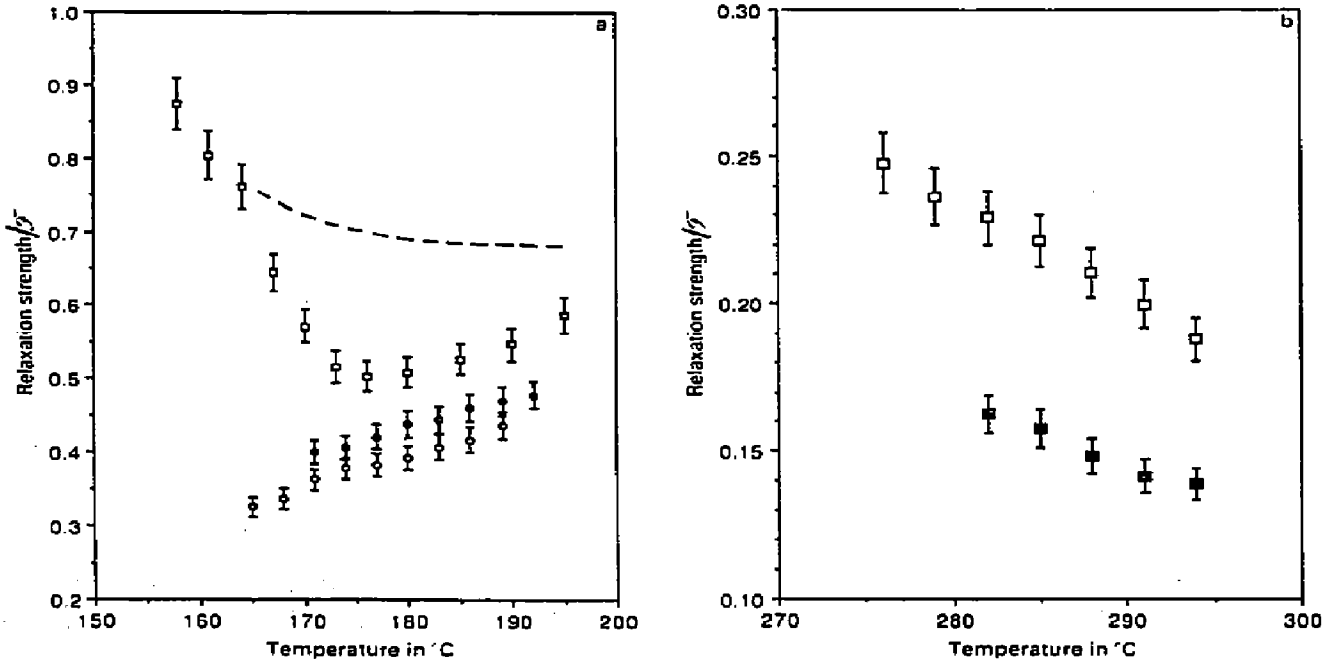

Fig. 11. Relaxation strength divided by field ratio as a function of temperature. (a) PEEK □, amorphous; ●, crystallized at 200°C; ○, crystallized at 280°C. The broken line represents an estimate of the behavior of completely uncrystallizable PEEK. (b) NEW-TPI: □, amorphous; ■, crystallized at 300°C.

Avrami exponent (from 2.8 to about 1.5 [33]), which usually is related to the formation of secondary crystals in a constrained geometry where fully three-dimensional growth is not considered possible. However, NEW-TPI exhibits no such change in kinetic processes: one Avrami exponent can be used to fit the entire crystallization curve [36]. Spherulitic growth has been observed to occur in NEW-TPI [41] and the Avrami exponent of $n = 3.5$ [36] is consistent with three-dimensional growth and a mixed nucleation process between athermal ($n = 3$) and thermal ($n = 4$) limiting cases [42]. However, the fact that a single process occurs over the entire range of crystallization times may mean that formation of secondary crystals is limited in NEW-TPI. This may be a consequence of its more rigid chemical structure and low chain mobility which may prevent nucleation of secondary crystals between the existing lamellae.

From the phase fractions shown in Fig. 3, we see that the degree of crystallinity is slightly smaller in NEW-TPI than in PEEK, but the amount of liquid-like amorphous phase is much greater and the amount of rigid, or constrained, amorphous phase is much smaller. In determining the phase fractions shown in Fig. 3, we utilized the method developed by Wunderlich's group [14–20]. At any temperature, the normalized heat capacity increment $\gamma(T)$ is defined as

$$\gamma(T) = \frac{C_p(T)^{sc}_{liquid} - C_p(T)^{sc}_{solid}}{C_p(T)^{a}_{liquid} - C_p(T)^{a}_{solid}} \tag{10}$$

where superscript sc represents the amorphous phase in the semicrystalline polymer, and superscript a represents the amorphous phase in the 100% amorphous polymer.

$\gamma(T_g)$ represents the total of mobile relaxing units, i.e. $\chi_a(T_g)$. As Mathot has shown, this is the fraction of the amorphous phase in the semicrystalline polymer which is able to exhibit cooperative glass transition relaxation behavior in the case where there is no excess heat capacity [43]. If the two-phase model is strictly valid and there is no excess heat capacity, then $\chi_c(T_g) = 1 - \gamma(T_g)$.

Wunderlich and co-workers [14–20] studied the thermal properties of several high-performance polymers as a function of processing history. This group showed that PEEK exhibits a rigid amorphous fraction which does not become liquid-like at the glass transition. In other words, this rigid material does not contribute to the distinct heat capacity increment at T_g. In the semicrystalline polymer, they found that the heat capacity increment decreased from its value in the amorphous sample far more than could be expected on the basis of the known degree of crystallinity. The rigid amorphous fraction behaves like the crystal fraction at T_g and was suggested to be located in the crystal/amorphous interphase region. It was also suggested that the rigid amorphous fraction might not become mobile until

the crystals themselves had melted [19, 20]. In the following sections we show that dielectric relaxation provides evidence that the rigid amorphous interphase fraction represents chains of reduced molecular mobility, and that these chains become mobile in the temperature range between T_g and T_m.

Dielectric properties

Dielectric relaxation is used to provide a more sensitive indicator of relaxation behavior in these two polymers. From the loss tangent data of Figs. 6 and 7 we see that in both PEEK and NEW-TPI, crystals serve to broaden the alpha relaxation (glass transition) and shift the tan δ peak to higher temperatures. The effect is very obvious in PEEK (Fig. 6) where two maxima are seen in the amorphous film which crystallizes during the heating. On the high temperature side, the tan δ peak does not decrease to the baseline because of the interference of a second higher temperature relaxation. Both polymers also show this second peak, which is the relaxation of the amorphous phase in the now crystalline material. The degree of separation of the two peaks depends upon the degree to which the crystals serve as constraints on the amorphous chains. In NEW-TPI, crystallization is relatively slow compared to PEEK and the glass transition temperature is hardly affected by the presence of the crystals. This results in the pronounced overlap of the two peaks. The peak position of tan δ is shifted to higher tempeature in the semicrystalline films (Fig. 7) and the peak width is increased on the high temperature side.

In spite of the fact that dielectric experiments are typically performed as a function of increasing temperature, it is not possible to analyze the temperature curves quantitatively. There is no simple relationship between peak height, or peak area, in temperature space, which would allow a direct connection to microscopic parameters. Therefore, the Cole–Cole plots are preferred because all frequency information is plotted together to obtain a single frequency-independent parameter, the relaxation strength. The parameter is directly related to microscopic variables through eqn. (5). Cole–Cole plots, such as those shown in Fig. 8, allow determination of ε_s, ε_∞, and the relaxation strength at any measurement temperature.

The limiting values of the dielectric constant, shown in Figs. 9 and 10, provide insight into the effects of the thermal history on relaxation processes occurring above the main glass transition relaxation. The high frequency value ε_∞ is controlled by sub-T_g processes in the amorphous phase. These motions involve localized dipole movements that do not require the large-scale mobility of amorphous polymer chain segments. For semicrystalline PEEK (Fig. 9(b)), ε_∞ is the same for samples which have identical mass fractions of liquid-like amorphous phase, but different mass fractions of crystallinity and rigid amorphous phase. Thus, from the

standpoint of localized motions, the crystals and the rigid amorphous phase can be grouped together. The data for ε_∞ for $T_c = 200°C$ overlap completely with the $T_c = 280°C$ data. The value of ε_∞ for the quenched amorphous PEEK (Fig. 9(a)) is very close to that of the semicrystalline samples, yet there are some differences. As the amorphous PEEK crystallizes, there is a sudden decrease in ε_∞. This is a result of the reduced number of amorphous phase dipoles which are available to contribute to the sub-T_g relaxation. After the sudden crystallization (from 165°C to about 175°C), the value of ε_∞ decreases faster with increasing temperature than the decrease seen in the two semicrystalline PEEK films. In NEW-TPI (Fig. 10), within the error limits, ε_∞ does not decrease with increasing temperature, and the data for the amorphous and semicrystalline materials overlap. We conclude that localized dipole movement in NEW-TPI is the same in the amorphous film as in the semicrystalline film.

In both PEEK and NEW-TPI, the low frequency, or static value, of the dielectric constant shows a strong dependence on structure. Samples with greater amorphous phase fractions have an increased value of ε_s. In Fig. 9(b), the PEEK film crystallized at 200°C has the greater value of ε_s compared to the film crystallized at 280°C. The two materials have the same liquid-like amorphous phase fractions from thermal analysis, but different rigid amorphous fractions and different degrees of crystallinity. Film with $T_c = 200°C$ has $\chi_c = 0.29$ and $\chi_{ra} = 0.30$, while film with $T_c = 280°C$ has $\chi_c = 0.35$ and $\chi_{ra} = 0.25$. The amorphous film (Fig. 9(a)) shows a decrease in ε_s with increasing temperature prior to crystallization. At 165°C, ε_s decreases sharply as the amorphous material is converted to the crystal phase. Above 175°C there is only a small decrease in ε_s, which is within the error bars. The values of ε_s after the amorphous film has crystallized are greater than either of the crystalline PEEK films over the temperature range, a reflection of the reduced degree of crystallinity in the quenched and now-crystalline film. NEW-TPI has the same trend between the semicrystalline film and amorphous film. Owing to the very slow cold crystallization process, there is no crystallization of the amorphous film up to 294°C. Therefore we conclude that the amorphous phase relaxes in the same manner in both the amorphous and semicrystalline NEW-TPI for the temperature range shown.

Relationship to microscopic parameters

The most significant information, and that which can be directly related to microscopic parameters through eqn. (6), is that shown in Fig. 11. The temperature dependence of $(\varepsilon_s - \varepsilon_\infty)/\mathcal{F}$ has several origins. As seen from eqn. (6), there is an explicit $1/T$ term arising from the temperature dependence of the orientational polarizability, which reduces the relaxation strength as a function of increasing temperature. This explicit temperature

dependence reflects the competition between thermal energy, which tends to misorient dipoles through thermal fluctuation, and the electric field energy which tends to align dipoles along the field direction. Of course, this term is always operational, and if there were no other temperature-dependent terms we would expect $(\varepsilon_s - \varepsilon_\infty)/\mathcal{F}$ always to decrease. In Fig. 11(a), the amorphous curve decreases prior to 165°C as a result of the thermal energy term. The decrease is steeper than a simple $1/T$ dependence, and this is usually interpreted as being due to the temperature dependence of the angular correlation of dipoles. Because the decrease is steeper than $1/T$, we conclude that cooperative interaction decreases with increasing temperature. In other words, in eqn. (6), orientational polarizability and $g(T)$ both exhibit the same trend, decreasing with increasing temperature. After 165°C, the amorphous curve decreases for these reasons, but also because of the sudden reduction in the number density of amorphous phase dipoles. As crystallization occurs from 166°C to 174°C, dipoles are removed from the amorphous phase, thus reducing N_r.

In this work we are concerned only with the relaxation process characterizing the glass transition in the amorphous phase of a polymer, so the relaxation strength, $(\varepsilon_s - \varepsilon_\infty)/\mathcal{F}$, relates specifically to amorphous phase behavior in 100% amorphous material. Then N_r refers to the number of amorphous phase dipole groups per unit of sample volume. Now consider what happens when the polymer of interest has a fractional degree of crystallinity χ_c. The number of amorphous phase dipole groups per unit of sample volume will be reduced, and the value of $(\varepsilon_s - \varepsilon_\infty)/\mathcal{F}$ will become $(1 - \chi_c)$ times its value in the 100% amorphous sample. From this we realize that any temperature-dependent process that alters the relative phase fractions (such as crystallization, melting, or liberation of constrained amorphous phase) will introduce temperature dependence into $(\varepsilon_s - \varepsilon_\infty)/\mathcal{F}$ through changes in N_r. We can now use the measured temperature dependence of $(\varepsilon_s - \varepsilon_\infty)/\mathcal{F}$ to deduce information about the temperature dependence of N_r.

Consistent with the reduced number density of amorphous phase dipoles, the semicrystalline samples (both PEEK and NEW-TPI) all have smaller values of $(\varepsilon_s - \varepsilon_\infty)/\mathcal{F}$ compared to the amorphous samples. The relaxation strength of NEW-TPI (Fig. 11(b)) is smaller than that of PEEK, probably as a result of the weaker permanent dipole, μ_r. However, the main difference between these two polymers is in the temperature dependence of $(\varepsilon_s - \varepsilon_\infty)/\mathcal{F}$ for the semicrystalline samples. In PEEK, the isothermally crystallized films, and the amorphous film after it has crystallized, show an *increase* in $(\varepsilon_s - \varepsilon_\infty)/\mathcal{F}$ as a function of temperature. This cannot be the result of any temperature dependency associated with orientational polarizability or correlated motion of dipoles, because these terms have the opposite trend. This increase in dielectric strength must come from temperature dependence in N_r. The reason for the increase in

N_r is the liberation of previously rigid amorphous phase dipoles, located at the crystal/amorphous interphase. These interphase dipoles, which surely have a distribution of molecular mobilities, are made mobile above the glass transition temperature of the liquid-like, or most mobile, amorphous phase dipoles.

As temperature increases (in spite of the countervening effects of thermal energy and dipole correlation which make $(\varepsilon_s - \varepsilon_\infty)/\mathcal{F}$ decrease), we still see strong increase in $(\varepsilon_s - \varepsilon_\infty)/\mathcal{F}$. This is true for all the crystalline PEEK and PPS samples we have studied [10, 11]. It is not true for NEW-TPI, however. As seen in Fig. 11(b), $(\varepsilon_s - \varepsilon_\infty)/\mathcal{F}$ for NEW-TPI decreases in both amorphous and semicrystalline films. We conclude that for this material, a very small amount of additional interphase dipoles are liberated for the range of temperatures studied. The temperature window is small, however, and efforts are currently underway to explore a lower temperature range closer to T_g for the semicrystalline NEW-TPI.

It is convenient to define a parameter, $\beta(T)$, which is the direct electrical analogue to $\gamma(T)$ from eqn. (10). We write a dielectric relaxation intensity ratio to represent the behavior of the amorphous phase in semicrystalline film normalized to its behavior in the 100% amorphous film. Thus, $\beta(T)$ is defined as

$$\beta(T) = [\Delta\varepsilon(T)^{sc}/\mathcal{F}^{sc}]/[\Delta\varepsilon(T)^{a}/\mathcal{F}^{a}] \tag{11}$$

where, as before, the superscript sc refers to the amorphous phase in the semicrystalline polymer, and superscript a refers to the amorphous phase in the 100% amorphous polymer. (The definition of $\beta(T)$ differs slightly from the one we used previously in which the terms containing $\mathcal{F}$ were omitted. This is justified because of the very weak temperature dependence of $\mathcal{F}$ but the present equation, eqn. (11), is more exact.) Comparing to eqn. (6), we now write

$$\beta(T) = N_r(T)^{sc}g(T)^{sc}/N_r(T)^{a}g(T)^{a} \tag{12}$$

If we assume that the dipole angular correlation term is approximately the same in the amorphous phase of both samples, then eqn. (12) simplifies further to

$$\beta(T) = N_r(T)^{sc}/N_r(T)^{a} \tag{13}$$

$\beta(T)$ represents the relative number of dipoles per unit volume which are relaxed at temperature T in the semicrystalline polymer, compared to the 100% amorphous polymer. This definition is convenient because it allows a direct comparison between the semicrystalline and 100% amorphous materials and provides an estimate of the effectiveness of crystals in constraining the mobility of amorphous chains.

Getting a precise value for $\beta(T)$ is difficult because evaluating the denominator of eqn. (11) from the data shown in Fig. 11 requires

TABLE 2

Lower and upper limiting values of $\beta(T)$ for PEEK [a] and NEW-TPI [b] compared to mobile amorphous, χ_a, and total amorphous, $\chi_{ra} + \chi_a$, mass fractions.

Material	T_{lower}/°C	$\beta(T_{lower})$	χ_a	T_{upper}/°C	$\beta(T_{upper})$	$\chi_{ra} + \chi_a$
PEEK	160	0.43	0.41	190	0.72	0.71
NEW-TPI	275	0.72	0.62	300	0.76	0.77

[a] PEEK cold-crystallized at 200°C. [b] NEW-TPI cold-crystallized at 300°C.

knowledge of the behavior of an amorphous sample at temperatures above T_g. PEEK polymer crystallizes so rapidly that we had to estimate the value of the denominator from an extrapolation of the amorphous data from temperatures above T_g to just below T_m. For PEEK this estimate uses the broken non-crystalline curve shown in Fig. 11(a). For NEW-TPI no extrapolation was required because the amorphous phase data overlap the crystalline sample data. In both cases, the values we find for $\beta(T)$ are estimates only.

In Table 2 we list selected estimated values of $\beta(T)$ for PEEK and NEW-TPI. If no rigid interphase dipoles are as yet relaxed, then at a temperature $T = T_{lower}$, $\beta(T)$ should be equal to the number of dipoles/volume in the liquid, or rubbery, state because only these dipoles contribute to the glass transition relaxation. From Table 2 we see that the estimated $\beta(T_{lower} = 160°C)$ for PEEK is nearly equal to χ_a, the liquid-like amorphous fraction determined from DSC. However for NEW-TPI, $\beta(T_{lower} = 275°C)$ is greater than χ_a. At an upper limit temperature, $T = T_{upper}$, if all rigid interphase is already relaxed, $\beta(T)$ should equal the total number/volume of amorphous phase dipoles because we expect the interphase to become mobile at the melting point. The temperature T_{upper} is chosen to be less than the onset temperature of the melting endotherm. In both polymers the upper limit $\beta(T_{upper})$ is nearly equal to $1 - \chi_c$ which is the total amorphous phase, including both χ_a and χ_{ra}. For PEEK, $\beta(T_{upper} = 190°C)$ is 0.72, and $\chi_{ra} + \chi_a$ is 0.71; in NEW-TPI, $\beta(T_{upper} = 300°C)$ is 0.76, and $\chi_{ra} + \chi_a$ is 0.77.

The physical interpretation of these results is the following. Above the DSC T_g, we expect all liquid-like amorphous phase to become mobile. But at T_{lower}, the rigid amorphous interphase has not yet become mobile. Thus, for PEEK $\beta(T_{lower})$ is very close in value to χ_a. The number density of dipoles relaxed just above the calorimetric T_g is about the same as the liquid-like amorphous fraction. However, in NEW-TPI $\beta(T_{lower})$ is greater than χ_a, indicating that a large portion of the interphase has already relaxed.

As temperature is increased, more and more dipoles from the rigid amorphous interphase join the relaxation. At the onset of melting, T_{upper}, all

TABLE 3

Ordering of polymers using chain flexibility, glass transition temperature and account of liquid-like amourphous phase present

	PBT < (most flexible)	PPS <	PEEK <	NEW-TPI (least flexible)
T_g/°C	35	90	145	249
χ_a	0.10	0.29	0.40	0.62

the rigid amorphous and liquid-like amorphous dipoles are relaxed in PEEK and NEW-TPI. Thus, $\beta(T_{upper})$ is very close to $\chi_a + \chi_{ra}$. The number density of dipoles relaxed by the onset of melting is about the same as the total amorphous fraction determined calorimetrically. We conclude that normalized dielectric relaxation intensity is a sensitive, quantitative indicator of the molecular mobility of the interphase regions.

The issue of the relationship between chain flexibility and formation of rigid amorphous material arises in considering other polymers, such as poly(butylene terephthalate), PBT. PBT has a very flexible chemical structure yet possesses almost no mobile morphous phase material, nearly all the amorphous phase being considered as rigid [19]. Clearly, the chemical structure differences that reduce chain flexibility, and increase the glass transition and melting point, are not the only factors that determine whether the amorphous phase will exhibit a rigid fraction. We suggest that the crystallization kinetics, and the formation of secondary crystallization, will be important factors that control the relative amount of rigid amorphous chains in PBT, PPS, PEEK and NEW-TPI. In terms of the qualitative estimate of chain flexibility, glass transition temperature, and amount of liquid-like amorphous phase, we would rank these polymers as shown in Table 3. The polymers that are least flexible have the greatest amount of mobile amorphous phase. However, on the basis of qualitative estimates of crystallization rate, and the amount of rigid amorphous phase present, the polymers would be ranked as shown in Table 4. The polymer with the most flexible chain (PBT) can crystallize the most rapidly, forming a large population of very poorly formed crystals that are effective in constraining the amorphous phase. NEW-TPI, which has the least flexible

TABLE 4

Order of polymers using crystallization rate and account of rigid amorphous phase present

	NEW-TPI < (slowest rate)	PEEK <	PPS <	PBT (fastest rate)
χ_{ra}	0.12	0.27	0.38	0.60

structure, crystallizes most slowly, and exhibits the least fraction of constrained amorphous phase chains.

This qualitative ordering is simply meant to suggest that it is inappropriate to say that stiffer chain polymers necessarily form the largest amount of rigid amorphous phase. The ability of crystals to act as constraints on the molecular mobility of the amorphous phase may be more directly related to the crystallization kinetics. In particular, polymers that crystallize rapidly and/or with a large fraction of secondary, in-filling lamellae, may be more effective in creating constrained amorphous chains. This picture is consistent with observations that crystallization under conditions of low chain mobility (such as cold crystallization, or crystallization by cooling at high rates) leads to formation of the greatest amount of constrained amorphous phase for a given polymer [11,20].

CONCLUSIONS

In this review, we have indicated how dielectric relaxation can be used as an important tool for the examination of structural relaxations in semicrystalline polymers. This tool shows excellent sensitivity to changes in microstructural parameters and allowed us to explore the relaxation of the crystal/amorphous interphase chains. The power of this technique is related to the direct association which can be made between the measured dielectric constant and loss in temperature–frequency space, and the microscopic parameters through well developed theoretical models. PEEK and NEW-TPI showed very different interphase relaxation behaviors above the glass transition. We suggest that these differences arise from differences in the crystallization behavior. Dielectric relaxation studies together with thermal analysis will lead to a better understanding of the role that chemical structure plays in determining the amount and nature of the constrained amorphous interphase.

ACKNOWLEDGMENTS

This research was supported by NSF-MRL (DMR87-19217). The authors thank Ingchie Kwan for assistance with thermal analysis.

REFERENCES

1 P.J. Flory, J. Am. Chem. Soc., 84 (1962) 2857.
2 R. Popli and R. Mandelkern, Polym. Bull., 9 (1983) 260.
3 P.J. Flory, D.Y. Yoon and K.A. Dill, Macromolecules, 17 (1984) 862.
4 D.Y. Yoon and P.J. Flory, Macromolecules, 17 (1984) 868.
5 R. Popli, M. Glotin, L. Mandelkern and R.S. Benson, J. Polym. Sci. Polym. Phys. Ed., 22 (1984) 407.
6 B. Hahn, J. Wendorff and D.J. Yoon, Macromolecules, 18 (1985) 718.

7 B. Hahn, O. Herrmann-Schonherr and J.H. Wendorff, Polymer, 28 (1987) 201.
8 K. Loufakis and B. Wunderlich, Macromolecules, 20 (1987) 2474.
9 J.D. Hoffman, G. Williams and E. Passaglia, J. Polym. Sci. Part C, 14 (1966) 173.
10 P.P. Huo and P. Cebe, J. Polym. Sci. Polym. Phys. Ed., 30 (1992) 239.
11 P.P. Huo and P. Cebe, Macromolecules, 25 (1992) 902.
12 P.P. Huo and P. Cebe, Polymer, 34(4) (1993) 696.
13 P.P. Huo and P. Cebe, Polymer, 33(23) (1992) 4913.
14 U. Gaur and B. Wunderlich, J. Phys. Chem. Ref. Data, 10 (1981) 119.
15 B. Wunderlich and G. Czornyi, Macromolecules, 10 (1977) 906.
16 S.-F. Lau and B. Wunderlich, J. Polym. Sci. Polym. Phys. Ed., 22 (1984) 379.
17 J. Grebowicz, S.F. Lau and B. Wunderlich, J. Polym. Sci. Polym. Symp., 71 (1984) 19.
18 H. Suzuki, J. Grebowicz and B. Wunderlich, Macromol. Chem., 186 (1985) 1109.
19 S.Z.D. Cheng, R. Pan and B. Wunderlich, Macromol. Chem., 189 (1988) 2443.
20 S.Z.D. Cheng, M.Y. Cao and B. Wunderlich, Macromolecules, 19 (1986) 1868.
21 H. Frohlich, Theory of Dielectrics, Oxford University Press, Oxford, 1949, p. 22.
22 N.G. McCrum, B.E. Read and G. Williams, Anelastic and Dielectric Effects in Polymeric Solids, John Wiley, New York, 1967, p. 82.
23 A.R. Blythe, Electrical Properties of Polymers, Cambridge University Press, Cambridge, 1979, p. 15.
24 C.C. Ku and R. Lupiens, Electrical Properties of Polymers: Chemical Principles, Hanser Publishers, Munich, 1987, p. 62.
25 R.T. Bailey, A.M. North and R.A. Pethrick, Molecular Motion in High Polymers, Oxford University Press, Oxford, 1981, p. 123.
26 S. Havriliak and S. Negami, Polymer, 8 (1967) 161.
27 P. Debye, Polar Molecules, Chemical Catalogue, New York, 1929.
28 R.H. Cole and K.S. Cole, J. Chem. Phys., 9 (1941) 341.
29 L. Onsager, J. Am. Chem. Soc., 58 (1936) 1486.
30 R.H. Boyd, J. Polym. Sci. Polym. Phys. Ed., 21 (1983) 505.
31 P.R. Bevington, Data Reduction and Error Analysis for the Physical Science, McGraw Hill, New York, 1969, p. 204.
32 D.J. Blundell and B.N. Osborn, Polymer, 24 (1984) 953.
33 P. Cebe and S.-D. Hong, Polymer, 27 (1986) 1183.
34 P.M. Hergenrother, SPE Conference on High Temperature Polymers and their Uses, Case Western Reserve University, October 2–4, 1989, Society of Plastics Engineers, Brookfield, CT.
35 J.B. Friler and P. Cebe, Polym. Sci. Eng., 33(10) (1993) 587.
36 P.P. Huo, J.B. Friler and P. Cebe, Polymer, 34(21) (1993) 4387.
37 Technical data sheet/A00, NEW-TPI, Mitsui-Toatsu Co.
38 P. Cebe, J. Mater. Sci., 23 (1988) 3721.
39 M. Avrami, J. Chem. Phys., 7 (1939) 1103.
40 M. Avrami, J. Chem. Phys., 8 (1940) 212.
41 S. Yuasa, M. Truji and T. Takahashi, Polym. Preprints (Jpn.), 40(1–4) (1991) 491.
42 B. Wunderlich, Macromolecular Physics, Vol. 2, Academic Press, New York, 1976, p. 147.
43 V.B.F. Mathot, Thermal characterization of states of matter, in Calorimetry and Thermal Analysis on Polymers, V.B.F. Mathot (Ed.), Hanser Publishers, Munich, 1993.